Slow-wave resonance in periodic stacks of anisotropic layers

Alex Figotin and Ilya Vitebskiy
Department of Mathematics, University of California at Irvine, Irvine, California 92697, USA
(Received 11 July 2007; published 30 November 2007)

We consider a Fabry-Perot resonance (a transmission band edge resonance) in periodic layered structures involving birefringent layers. In a previous publication [Phys. Rev. E **72**, 036619 (2005)] we have shown that the presence of birefringent layers with misaligned in-plane anisotropy can dramatically enhance the performance of the photonic-crystal resonator. It allows us to reduce its size by an order of magnitude without compromising on its performance. The key characteristic of the enhanced slow-wave resonator is that the Bloch dispersion relation $\omega(k)$ of the periodic structure displays a degenerate photonic band edge, in the vicinity of which the dispersion curve can be approximated as $\Delta\omega \sim (\Delta k)^4$, rather than $\Delta\omega \sim (\Delta k)^2$. Such a situation can be realized in specially arranged stacks of misaligned anisotropic layers. On the down side, the presence of birefringent layers results in the slow-wave resonance being coupled only with one (elliptic) polarization component of the incident wave, while the other polarization component is reflected back to space. In this paper we show how a small modification of the periodic layered array can solve the above fundamental problem and provide a perfect impedance match regardless of the incident wave polarization, while preserving the giant slow-wave resonance characteristic of a degenerate photonic band edge. Both features are of critical importance for many practical applications, such as the enhancement of various light-matter interactions, light amplification and lasing, optical and microwave filters, antennas, etc.

DOI: 10.1103/PhysRevA.76.053839 PACS number(s): 42.70.Qs, 78.66.Fd

I. INTRODUCTION

Wave propagation in spatially periodic media, such as photonic crystals, can be qualitatively different from any uniform substance. The differences are particularly pronounced when the wavelength is comparable to the primitive translation L of the periodic structure [1–7]. The effects of strong spatial dispersion culminate at stationary points $\omega_s = \omega(k_s)$ of the Bloch dispersion relation where the group velocity $u = \partial\omega/\partial k$ of a traveling Bloch wave vanishes

$$\frac{\partial \omega}{\partial k} = 0, \quad \text{at } k = k_s, \quad \omega = \omega_s = \omega(k_s). \tag{1}$$

One reason for this is that vanishing group velocity always implies a dramatic increase in density of modes at the respective frequency. In addition, vanishing group velocity also implies certain qualitative changes in the eigenmode structure, which can be accompanied by some spectacular effects in wave propagation. A particular example of the kind is the frozen mode regime associated with a dramatic amplitude enhancement of the wave transmitted to the periodic medium [8–13]. In this paper, we focus on a different slow-wave effect, namely, on a Fabry-Perot resonance in bounded photonic crystals. This slow wave phenomenon, illustrated in Figs. 1 and 2, is also referred to as the transmission band edge resonance. There are some similarities between the frozen mode regime and the slow-wave resonance in plane-parallel photonic crystals. Both effects are associated with vanishing group velocity at stationary point (1) of the Bloch dispersion relation. As a consequence, both effects are strongly dependent on specific type of spectral singularity (1). A fundamental difference though is that the frozen mode regime is not a resonance phenomenon in the sense that it is not particularly sensitive to the shape and size of the photonic crystal. For instance, the frozen mode regime can occur even in a semi-infinite periodic structure, where the incident plane wave is converted to a frozen mode slowly propagating through the periodic medium until it is absorbed [8–13]. By contrast, in the case of a slow-wave resonance, the entire bounded periodic structure acts as a resonator, resulting in a strong sensitivity of the resonance behavior to the size and shape of the photonic crystal.

It is also important to distinguish between two qualitatively different classes of photonic-crystal resonators. The first class comprises resonance cavities where the role of periodic dielectric structure reduces to electromagnetic (EM) field confinement by reflecting it back to the cavity interior. The resonance frequency (or frequencies) of such photonic cavities usually lies in a frequency gap (a stop band) of the photonic crystal. The periodic dielectric array here plays the

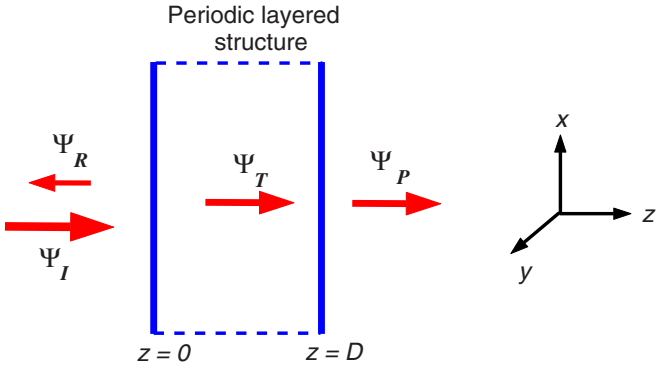

FIG. 1. (Color online) Scattering problem of a plane wave normally incident on a periodic stack of dielectric layers. The indices I, R, and P denote the incident, reflected, and transmitted waves, respectively. The field inside the periodic medium is Ψ_T. In the case of a slow wave resonance, the incident wave frequency lies in a transmission band of the periodic structure, close to a band edge, as illustrated in Fig. 2.

 ©2007 The American Physical Society

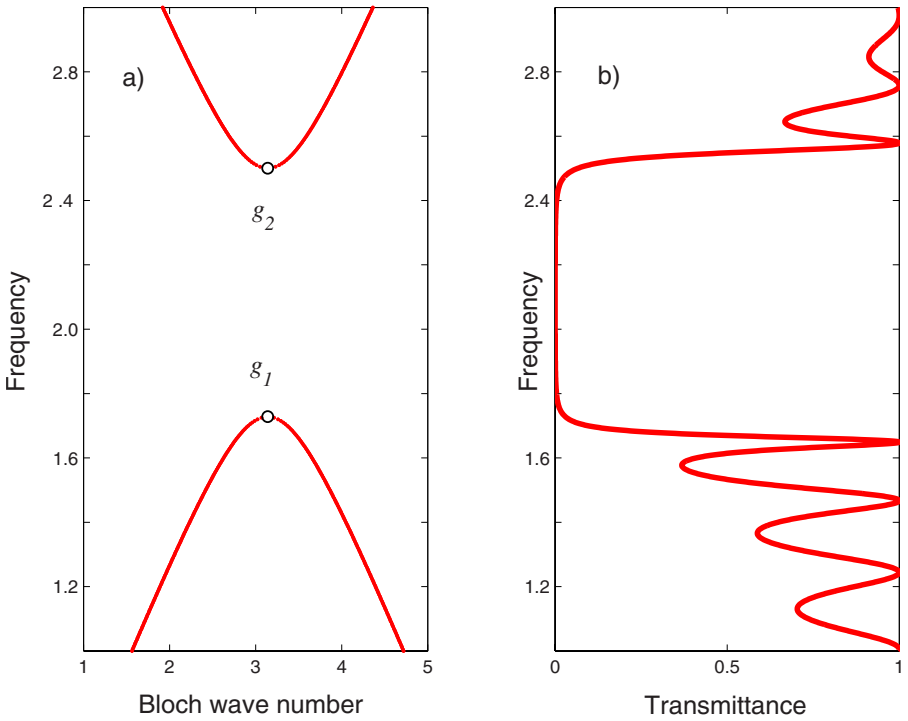

FIG. 2. (Color online) (a) A fragment of a typical Bloch k-ω diagram of a periodic array composed of nonbirefringent layers; g_1 and g_2 are the edges of the lowest photonic band gap. Each spectral branch is doubly degenerate with respect to the wave polarization. (b) Transmission dispersion $t(\omega)$ of the respective finite periodic stack; the sharp peaks near the edges of the transmission bands are associated with slow-wave Fabry-Perot resonances, also known as transmission band edge resonances. The location (6) of the resonance peaks depends on the number N of unit cells L in the periodic stack. Wave number k and frequency ω are expressed in units of L^{-1} and cL^{-1}, respectively.

role of a distributed Bragg reflector. The number of resonance modes depends on the cavity size. It can be a single mode localized on an isolated defect inside the photonic crystal [14,15]. Or the cavity can support multiple resonances, if its size significantly exceeds the light wavelength. More detailed information on photonic crystal cavities can be found in numerous papers and monographs on optics and photonics (see, for example, Ref. [16], and references therein). In this paper, we will not further discuss this subject.

The second class of photonic-crystal resonators comprises the so-called slow-wave resonators. They are qualitatively different from the band-gap cavities. In slow-wave photonic-crystal resonators, the reflectors may not be needed at all, as shown in the example in Fig. 1. The role of the periodic structure here is to support slow EM waves. The resonance frequencies lie in the transmission bands of the photonic crystal—not in band gaps, although, they can be very close to a band edge (1), as shown in Fig. 2. A typical example of slow wave resonance in a photonic crystal is presented by the transmission band edge resonance, illustrated in Figs. 1 and 2. In certain cases, slow-wave resonators can provide significant advantages over cavity resonators. They are used for the enhancement of light-matter interactions, such as nonlinear and nonreciprocal effects, optical activity, light amplification and lasing, etc. They can also be used in optical and microwave filters, delay lines, as well as for the enhancement of antenna gain and directionality. More detailed information can be found in the extensive literature on the subject (see, for example, Refs. [4–6,17–22], and references therein).

In this paper we describe a slow-wave photonic-crystal resonator with drastically reduced dimensions and enhanced performance, compared to that of a common Fabry-Perot resonator based on a periodic stack of nonbirefringent layers. The idea is to employ periodic structures supporting the dispersion relations different from those allowed in periodic arrays of nonbirefringent layers. Indeed, periodic arrays involving birefringent layers can display stationary points (1) different from a regular photonic band edge in Fig. 2(a). Some examples are shown in Fig. 3. Slow waves associated with such stationary points can produce giant transmission band-edge resonances, much more powerful compared to those achievable in common layered structures. The first step in this direction was made in Ref. [23], where it was shown that the transmission band-edge resonance in the vicinity of a degenerate photonic band edge (DBE) in Fig. 3(b) produces much better results, compared to a regular photonic band edge (RBE) of Figs. 2(a) and 3(a). Specifically, at the frequency of DBE related giant slow-wave resonance, the electromagnetic energy density inside the photonic-crystal can be estimated as

$$\langle W_{\mathrm{DBE}} \rangle \propto W_I N^4, \tag{2}$$

where W_I is the energy density of the incident wave and N is the total number of unit cells in the periodic stack. By comparison, the average EM energy density at a regular transmission band-edge resonance in Fig. 2 is

$$\langle W_{\mathrm{RBE}} \rangle \propto W_I N^2. \tag{3}$$

The estimations (2) and (3) imply that the Q factor of a DBE-based slow-wave resonator can be by factor N^2 higher compared to that of a RBE related Fabry-Perot resonator of the same size; this a huge difference. A detailed comparative analysis of the giant DBE related slow-wave resonance versus the regular transmission band edge resonance can be found in Ref. [23].

On the down side, periodic structures with birefringent layers have a fundamental problem—their reflectance and transmittance are essentially dependent on the incident wave

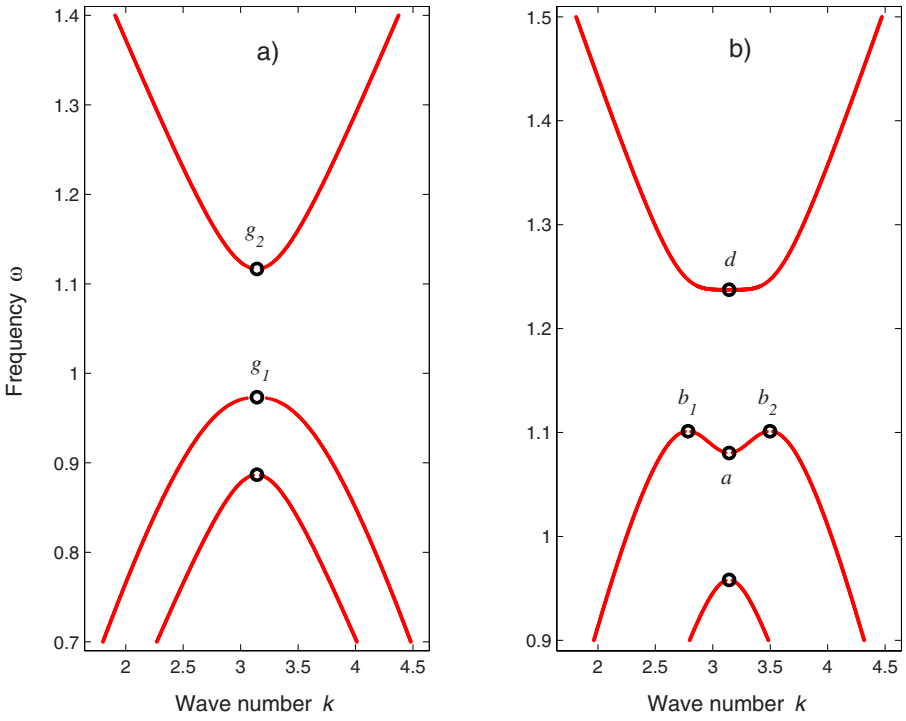

FIG. 3. (Color online) Fragments of the k-ω diagrams of the periodic layered structure in Fig. 6 for two different values of the ratio A/B of the layer thicknesses. Regular, degenerate, and split photonic band edges are denoted by symbols g, d, and b, respectively. The Bloch wave number k and the frequency ω are expressed in units of $1/L$ and c/L.

polarization. This dependence is particularly strong near the edges of transmission bands, where the slow-wave resonances occur. In particular, a DBE related giant transmission resonance described in Ref. [23] is coupled only with one (elliptic) polarization component of the incident wave, while the other polarization component is reflected back to space by the photonic crystal boundary [23]. In other words, at the resonance frequency, a periodic stack involving birefringent layers acts as a polarizer, reflecting back to space roughly half of the incident wave energy. This behavior is illustrated in Figs. 4 and 5. Similar problem exists in all different modifications of the frozen mode regime considered in Refs. [8–13]. For many applications, such a polarization selectivity may not be acceptable. In this paper we offer a solution to the above problem. We show how to utilize all the incident wave energy, while preserving the extraordinary performance of the DBE based photonic-crystal resonator. The idea is to modify the periodic layered array so that instead of a degenerate band edge, the respective dispersion curve develops a split photonic band edge (SBE) shown in Fig. 3(b). Under certain conditions specified below, the photonic resonator with a SBE will display a giant transmission band edge resonance, similar to that of a DBE. But, in addition, the SBE resonator couples with the incident wave regardless of its polarization and, therefore, utilizes all the incident EM radiation—not just one polarization component. The latter feature is of critical importance for a variety of practical applications. Similar approach can be applied not only to a photonic-crystal cavity resonance, but also to all different modifications of the frozen mode regime described in Refs. [8–13].

II. GEOMETRICAL DESCRIPTION OF SLOW-WAVE RESONANCE

Steady-state Fabry-Perot resonance in a plane-parallel photonic crystal is commonly described as a standing Bloch wave composed of a pair of reciprocal propagating Bloch modes with equal and opposite wave numbers and group velocities

$$\Psi_T(z) = \Psi_k(z) + \Psi_{-k}(z), \quad 0 < z < D. \tag{4}$$

At a resonance, the two propagating Bloch components in Eq. (4) have large and nearly equal amplitudes and low group velocities. Two nodes of the standing wave coincide with the photonic crystal boundaries at $z=0$ and $z=D$, which determines the resonance values k_m of the Bloch wave number k

$$k_m \approx k_0 \pm \frac{\pi}{NL} m, \quad m = 1,2, \ldots, \tag{5}$$

where k_0 coincides with one of stationary points (1) of the dispersion relation $\omega(k)$ (usually, $k_0=0$ or π). The integer m denotes the resonance peaks in order of their distance from the respective photonic band edge at k_0. The resonance frequencies ω_m are expressed in terms of the Bloch dispersion relation

$$\omega_m = \omega(k_m), \tag{6}$$

and located close to the photonic band edge at $\omega_0=\omega(k_0)$. According to Eq. (5), the proximity of the resonances to the photonic band edge is determined by the number N of unit cells in the periodic stack. The expressions (5) and (6) only apply if

$$N \gg m. \tag{7}$$

The simple representation (4) for the resonance field distribution works very well in the vicinity of a regular photonic band edge (RBE). In the case of a giant transmission resonance associated with a degenerate photonic band edge (DBE), the above simple picture does not apply. Indeed, ac-

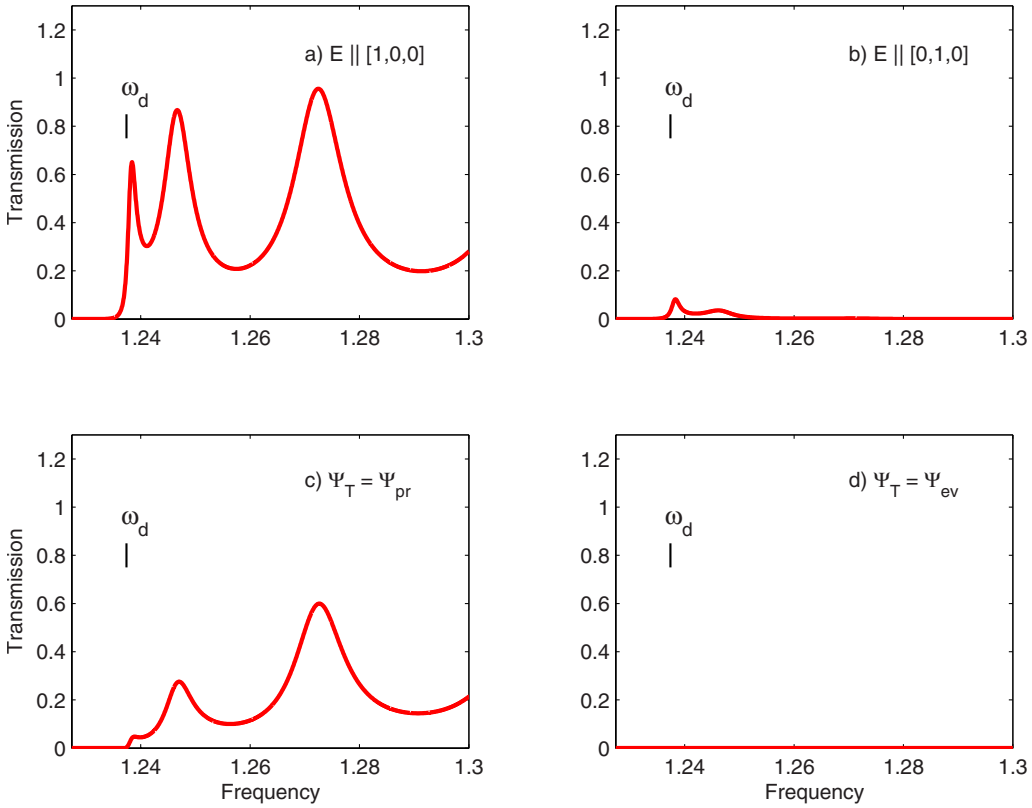

FIG. 4. (Color online) Transmission dispersion of the periodic stack of 18 unit cells at frequency range including the DBE at $\omega=\omega_d$. The respective k-ω diagram is shown in Fig. 3(b). In the cases (a) and (b), the incident wave in linearly polarized. In the cases (c) and (d), the incident wave polarization is adjusted so that at any given frequency it corresponds to a single mode excitation regime: in the case (c) it is a single propagating mode, while in the case (d) it is a single evanescent mode. Obviously, in the latter case the incident wave is reflected back to space. The frequency ω is expressed in units of cL^{-1}.

cording to Ref. [23], in the vicinity of a DBE, the evanescent mode contribution becomes equally important, and the resonance field $\Psi_T(z)$ cannot be viewed as a simple standing Bloch wave (4). Yet another qualitatively different situation can occur in the vicinity of a split photonic band edge (SBE), provided that the magnitude of the split between the edges b_1 and b_2 in Fig. 3(b) is small enough so that the respective SBE is close in shape to a DBE. In this latter case, a giant transmission resonance (2) is produced by interference of two pairs of reciprocal propagating Bloch waves

$$\Psi_T(z) = \Psi_A(z) + \Psi_B(z), \quad 0 < z < D, \tag{8}$$

where

$$\Psi_A(z) = \Psi_{k_A}(z) + \Psi_{-k_A}(z) \tag{9}$$

and

$$\Psi_B(z) = \Psi_{k_B}(z) + \Psi_{-k_B}(z). \tag{10}$$

Either a DBE or a SBE can only exist in periodic stacks involving misaligned birefringent layers, example of which is shown in Fig. 6. The same photonic crystal can develop both a DBE and a SBE at different frequencies, as shown in Fig. 3(b). Either of them can produce a giant transmission resonance (2). The difference, though, is that a DBE related giant transmission resonance is coupled with only one of the two polarization components of the incident light [13,23], as shown in Figs. 4 and 5. By contrast, an equally powerful RBE related transmission resonance can be polarization independent, as illustrated in Figs. 7 and 8. The latter feature is a significant advantage for most applications.

For simplicity, in further consideration we restrict ourselves to the case of a plane monochromatic wave normally incident on a layered structure, as shown in Fig. 1. The results can be easily generalized to the case of oblique incidence, as it was done, for example, in Refs. [9,13]. Basic notations and definitions of electrodynamics of stratified media involving birefringent layers are explained in Appendix A. Similar notations and terminology are used, for instance, in Refs. [8,9,13,23].

A. Transmission band-edge resonance in the vicinity of a split photonic band edge

Consider the vicinity of a split photonic band edge (SBE) on the k-ω diagram in Fig. 3(b). The physical characteristics of the periodic structure are chosen so that the SBE in Fig. 3(b) is close in shape to a DBE. The frequency range

$$\omega_0 < \omega < \omega_b, \tag{11}$$

covers a narrow portion of the transmission band which includes the SBE. At any given frequency from Eq. (11), there

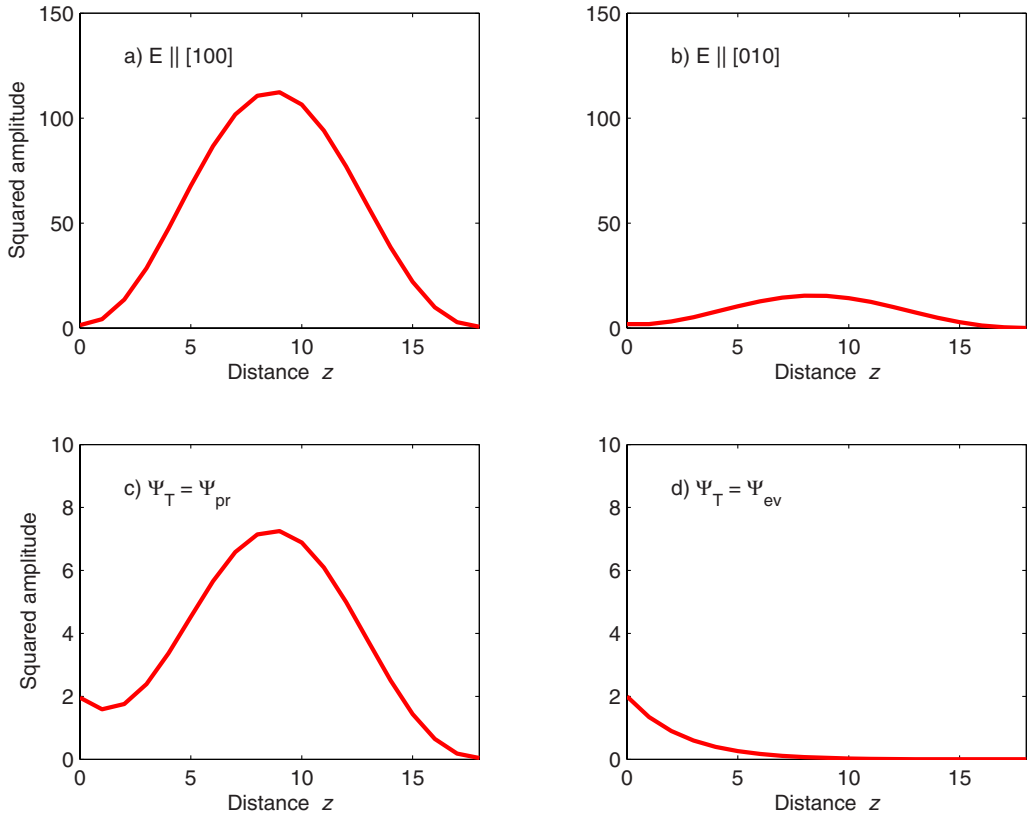

FIG. 5. (Color online)Smoothed energy density distribution $W(z)$ at frequency of the first (closest to the DBE) giant transmission band edge resonance in Fig. 4 for four different polarizations of the incident wave. In a single mode excitation regime of (c) and (d), the transmission resonance is suppressed. Particularly so in the case (d), where the EM field inside the periodic medium corresponds to a single evanescent mode. The distance z is expressed in units of L.

are two pairs of reciprocal Bloch waves with very low group velocity and different polarizations; each pair being capable of producing its own slow-wave cavity resonance with the resonance conditions similar to Eq. (5). Our focus is on the possibility of the two resonances occurring at the same frequency. Such a situation will be referred to as the double resonance. It turns out that the double transmission band edge resonance is as powerful as the giant resonance associated with a DBE. However, in addition, a SBE related resonance utilizes all the energy of the incident wave regardless of its polarization. By contrast, a DBE based giant transmission resonance is coupled only with one polarization component of the incident wave; the rest of the incident wave energy being reflected back to space. This important difference is obvious if we compare the DBE related transmission dispersion shown Fig. 4 and the SBE related transmission dispersion shown in Fig. 7.

Let us introduce the following dimensionless notations for the small deviation of the wave number and the frequency from the respective stationary point:

$$\kappa = |k - k_0|L, \quad \nu(\kappa) = [\omega(k) - \omega(k_0)]L/c. \tag{12}$$

According to Eqs. (5) and (6), the resonance values of κ and ν are

$$\kappa_m \approx \frac{\pi}{N} m \ll 1, \quad \nu_m \approx \nu(\kappa_m). \tag{13}$$

The most powerful resonance is usually the one closest to the respective photonic band edge

$$\kappa_1 \approx \frac{\pi}{N} \ll 1, \quad \nu_1 \approx \nu(\kappa_1). \tag{14}$$

Let us now consider a dispersion curve with a SBE in more detail. If the split between the twin band edges b_1 and

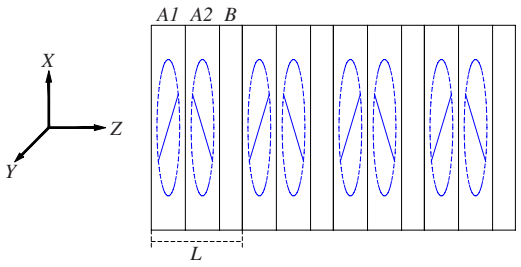

FIG. 6. (Color online) Periodic layered structure with a unit cell L containing two misaligned anisotropic A layers, and one isotropic B layer. The respective dielectric permittivity tensors are given in Eqs. (B1), (B2), and (B4). This is the simplest layered array supporting the Bloch dispersion relation with a DBE and/or a SBE, as shown in Fig. 3(b).

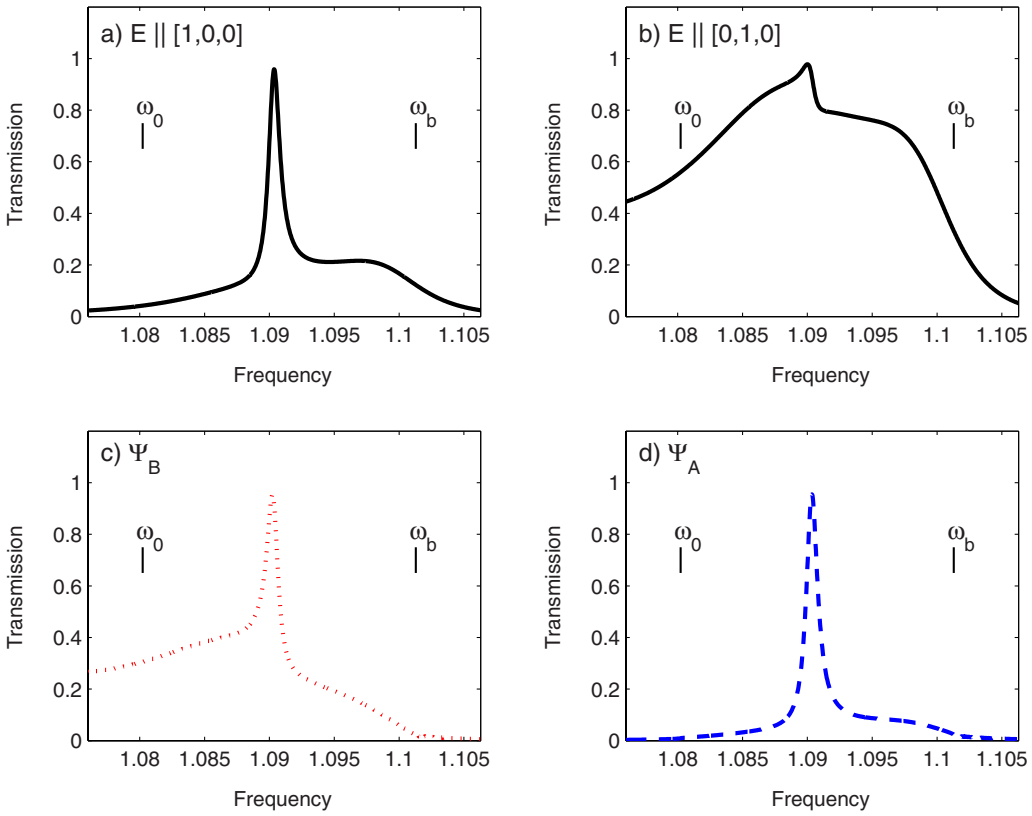

FIG. 7. (Color online) Manifestation of SBE related double resonance in the transmission dispersion $t(\omega)$ of periodic stack with $N=18$. The respective k-ω diagram is shown in Fig. 3(b). Observe that at the resonance frequency, the stack transmittance is close to unity regardless of the incident wave polarization. By contrast, in the case of DBE-related giant transmission resonance in Fig. 4, the impedance matching is polarization dependent. In the cases (c) and (d), the incident wave polarization is adjusted so that at any given frequency it would excite a single propagating Bloch mode (Ψ_A or Ψ_B) in the respective semi-infinite layered structure. The frequency ω is expressed in units of cL^{-1}.

b_2 in Figs. 3(b) is small, the dispersion relation in the vicinity of SBE can be approximated as

$$\nu(\kappa) \approx \frac{a}{2}\kappa^2 + \frac{b}{4}\kappa^4, \tag{15}$$

where

$$a/b < 0 \tag{16}$$

and

$$|a/b| \ll 1. \tag{17}$$

The inequality (16) is the condition for SBE. Indeed, in the opposite case of

$$a/b > 0, \tag{18}$$

the dispersion curve (15) would develop a RBE at $\kappa=0$, as shown in Fig. 3(a). While in the case

$$a/b = 0, \tag{19}$$

the dispersion curve (15) would have a DBE at $\kappa=0$. The additional inequality (17) is the condition for the proximity of the SBE to a DBE. This proximity allows us to use the expansion (15) in the frequency range spanning both twin edges of the SBE. More importantly, the condition (17) is essential for the phenomenon of the giant transmission resonance in the vicinity of SBE.

There are three stationary points associated with a SBE. The first one is trivial

$$\kappa_a = 0, \quad \nu_a = 0. \tag{20}$$

It is located either at the center of the Brillouin zone, or at its boundary. The other two stationary points correspond to the actual SBE

$$\pm\kappa_b = \pm\sqrt{-a/b}, \quad \nu_b = -a^2/4b. \tag{21}$$

Taking into account Eq. (21), the condition (17) for the proximity of the SBE to a DBE can be recast as

$$\kappa_b \ll 1. \tag{22}$$

The condition (22) implies that the points b_1 and b_2 on the dispersion curve are close to each other.

In what follows, we assume for simplicity that

$$b < 0 < a. \tag{23}$$

In this case, the SBE in question corresponds to the upper edge of the transmission band, as shown in Fig. 3(b). The alternative case of

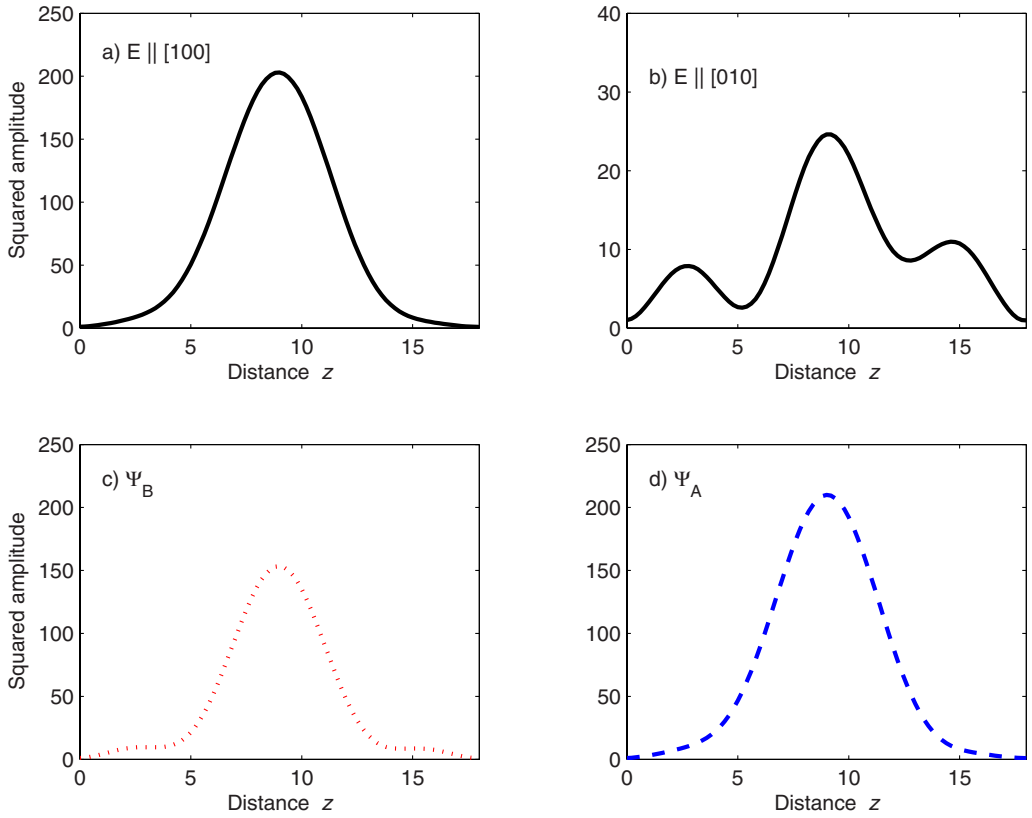

FIG. 8. (Color online) Smoothed energy density distribution at frequency of the SBE related giant transmission resonance in Fig. 7 for four different polarizations of the incident wave. The cases (c) and (d) relate to a single mode excitation regime. The distance z is expressed in units of L.

$$a < 0 < b \tag{24}$$

corresponds to the SBE being the lower edge of the respective transmission band. There is no qualitative difference between the two cases.

At any given frequency ν within the range

$$\nu_a < \nu < \nu_b, \tag{25}$$

there are two pairs (9) and (10) of reciprocal Bloch waves. Each pair comprises one forward and one backward propagating modes with equal and opposite wave numbers and group velocities

$$\pm\kappa_A = \pm\kappa_b\sqrt{1-\sqrt{1-\frac{\nu}{\nu_b}}}, \quad \nu_a < \nu < \nu_b, \tag{26}$$

$$\pm\kappa_B = \pm\kappa_b\sqrt{1+\sqrt{1-\frac{\nu}{\nu_b}}}, \quad \nu < \nu_b. \tag{27}$$

The pair of wave numbers (26) corresponds to the concave portion of the dispersion curve (15), while the pair of wave numbers (27) corresponds to the convex portion of the dispersion curve. Obviously,

$$\kappa_A < \kappa_B \quad \text{at } \nu_a < \nu < \nu_b. \tag{28}$$

B. Conditions for the double SBE resonance

Within the frequency range (25), either pair of the reciprocal Bloch waves (9) and (10) can develop a transmission resonance. Of particular interest here is the case where the two resonances occurs at the same or almost the same frequency. This situation is illustrated in Fig. 9(c), as well as in Figs. 7 and 8.

Let us start with the resonance created by the reciprocal pair (9) of Bloch waves corresponding to the concave section of the dispersion curve in Fig. 3(b). It is possible that the frequency range (25) contains only a single cavity resonance—the one with $m=1$. Such a case is determined by either the proximity of the SBE to a DBE, or by the right choice of the number N of the unit cells in the stack. According to Eqs. (21) and (5), the condition for a single resonance is

$$\kappa_1 < \kappa_b < 2\kappa_1, \quad \kappa_A = \kappa_1 = \frac{\pi}{N}. \tag{29}$$

The respective resonance frequency ν_A is determined by Eqs. (6) and (15)

$$\nu_A = \nu_1 = \frac{a}{2}\kappa_1^2 + \frac{b}{4}\kappa_1^4, \tag{30}$$

where $\kappa_1 = \pi/N$.

Consider now the resonance created by the reciprocal pair (10) of Bloch waves corresponding to the convex section of

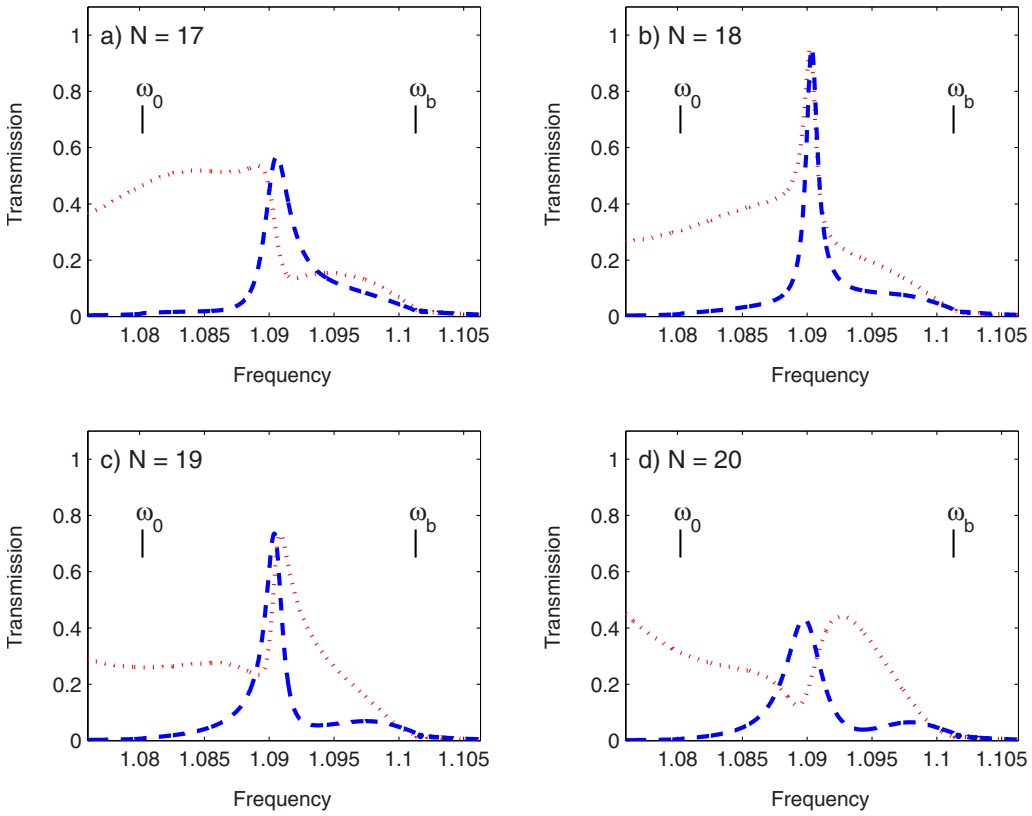

FIG. 9. (Color online) Transmission dispersion of periodic stacks composed of different number N of unit cells. The frequency range shown includes SBE on the k-ω diagram in Fig. 3(b). The two curves correspond to two different polarizations of incident wave. In either case, at any given frequency ω, the incident wave polarization is adjusted so that it would excite a single propagating Bloch mode (Ψ_A or Ψ_B) in the respective semi-infinite periodic structure. In the case (b) of $N=18$, the two resonance frequencies nearly coincide, creating condition for double transmission resonance with perfect impedance matching. The frequency ω is expressed in units of cL^{-1}.

the dispersion curve. Let us impose the condition

$$\nu_A = \nu_B \equiv \nu_r \tag{31}$$

that both resonances occur at the same frequency (30). This condition leads to the following equality:

$$\frac{a}{2}\kappa_A^2 + \frac{b}{4}\kappa_A^4 = \frac{a}{2}\kappa_B^2 + \frac{b}{4}\kappa_B^4.$$

Simple analysis shows that it is only possible if at $\nu=\nu_r$ we have

$$\kappa_A = 2\kappa_B = 2\kappa_1 = \frac{2\pi}{N}.$$

The relation

$$\kappa_A = 2\kappa_B$$

together with Eqs. (26) and (27) yield

$$\kappa_b = \sqrt{\frac{5}{2}}\kappa_1 = \sqrt{\frac{5}{2}}\frac{\pi}{N}.$$

The frequency of the double transmission resonance is

$$v_r = \left(\frac{4}{5}\right)^2, \quad v_b = \frac{2}{5}b\left(\frac{\pi}{N}\right)^2. \tag{32}$$

The group velocities of the two reciprocal pairs of Bloch waves at the resonance frequency v_r are

$$u_A = \mp\frac{3}{2}b\kappa_1^3 = \mp\frac{3}{2}b\left(\frac{\pi}{N}\right)^3$$

and

$$u_B = \pm 3b\kappa_1^3 = \pm 3b\left(\frac{\pi}{N}\right)^3.$$

By comparison, in the case of a DBE related giant transmission band edge resonance, we would have the following estimation for the resonance frequency v_1 and the respective group velocity of the two propagating Bloch components

$$v_1 \propto \frac{b}{N^2}, \quad u_1 \propto \frac{b}{N^3}.$$

These estimations are similar to those related to the double transmission resonance associated with a SBE. In either case, the average resonance energy density is estimated by Eq. (3), which justifies the term "giant" transmission resonance.

Let us remark that the entire consideration of this subsection was based on the assumption that each pair (9) and (10)

of the reciprocal Bloch modes is responsible for its own individual transmission resonance, described as a standing wave (9) or (10), respectively. While the double resonance at ν_r is described as the situation where the frequencies ν_A and ν_B of those individual resonances merely coincide. In fact, these two transmission resonances can be treated as independent only if the respective resonance frequencies ν_A and ν_B are separated. As soon as ν_A and ν_B are close to each other, the contributions of all four propagating Bloch modes to the resonance field $\Psi_T(z)$ in Eq. (8) become equally important. The latter situation persists even if the incident wave polarization correspond to the, so-called, single mode excitation regime, defined in Refs. [13,23] for the case of a semi-infinite periodic structure. In other words, the single mode excitation regime produces almost pure $\Psi_A(z)$ resonance (9) or $\Psi_B(z)$ resonance (10) only if their frequencies are well separated. Otherwise, the EM field $\Psi_T(z)$ is a superposition of all four Bloch eigenmodes. In such a case, the resonance field $\Psi_T(z)$ cannot be viewed as a simple standing wave (4) regardless of the incident wave polarization. The physical reason for such a strong hybridization is that due to the condition (22), the RBE in question is very close to a DBE. On the other hand, in the vicinity of a DBE, all four vector columns $\Psi_k(z)$ in Eq. (A4) become nearly parallel to each other [13,23]. The latter circumstance excludes the possibility of exciting only one of the two pairs of the reciprocal Bloch modes (9) or (10) in the situation (31), where the resonance conditions (5) are in place for both of them simultaneously. Still, the above consideration provides a very useful guidance on the conditions for SBE related giant transmission resonance and allows to find the proper physical characteristics of the periodic structure.

The bottom line is that the SBE related giant transmission resonance is as powerful as that related to a DBE. However, in addition, the SBE related resonance provides a perfect coupling with the incident wave regardless of its polarization.

III. CONCLUSION

In summary, we would like to stress that the remarkable features of the DBE and SBE related giant transmission resonances can be derived from such fundamental characteristics of the periodic composite medium as its electromagnetic dispersion relation. Specific details of the periodic array, such as physical characteristics of the constitutive components, or structural geometry, are only important as long as the symmetry of the periodic array is compatible with the existence of the required spectral singularities.

ACKNOWLEDGMENTS

Effort of A. Figotin and I. Vitebskiy is sponsored by the Air Force Office of Scientific Research, Air Force Materials Command, USAF, under Grant No. FA9550-04-1-0359. The authors are thankful to A. Chabanov for stimulating discussions.

APPENDIX A: ELECTRODYNAMICS OF STACKS OF BIREFRINGENT LAYERS

In this appendix we briefly introduce some basic notations and definitions of electrodynamics of stratified media involving birefringent layers. A detailed and consistent description of the subject, along with numerous references, can be found in Refs. [8,9,13,23], where similar notations and terminology are used. For simplicity, we restrict ourselves to the case of a plane monochromatic wave normally incident on a layered structure, as shown in Fig. 1. The results can be easily generalized to the case of oblique incidence, as was done, for example, in Refs. [9,13].

Time-harmonic electromagnetic field inside and outside the layered medium can be described by the vector column

$$\Psi(z) = \begin{bmatrix} E_x(z) \\ E_y(z) \\ H_x(z) \\ H_y(z) \end{bmatrix}, \tag{A1}$$

where $\vec{E}(z)$ and $\vec{H}(z)$ are time-harmonic electric and magnetic fields. The z direction is normal to the layers. The values of Ψ at any two locations z and z' are related by the transfer matrix $T(z,z')$ defined by

$$\Psi(z) = T(z,z')\Psi(z'). \tag{A2}$$

The elements of the transfer matrix are expressed in terms of material tensors and other physical characteristics of the stratified medium.

Let Ψ_I, Ψ_R, and Ψ_P be the incident, reflected, and transmitted waves, respectively, as shown in Fig. 1. To the left of the stack (at $z<0$), the electromagnetic field is a superposition of the incident and reflected waves. To the right of the stack (at $z>D$), there is only the transmitted wave. The field inside the periodic medium is denoted as Ψ_T. All four transverse field components in Eq. (A1) are continuous functions of z, which produces the following boundary conditions at $z=0$ and $z=D$ in Fig. 1:

$$\Psi_I(0) + \Psi_R(0) = \Psi_T(0), \quad \Psi_P(D) = \Psi_T(D). \tag{A3}$$

Inside the periodic stratified medium, at any given frequency ω, the time-harmonic field $\Psi_T(z)$ can be represented as a superposition

$$\Psi_T(z) = \Psi_{k1}(z) + \Psi_{k2}(z) + \Psi_{k3}(z) + \Psi_{k4}(z), \quad 0 < z < D \tag{A4}$$

of four Bloch eigenmodes, each of which satisfies the following relation:

$$\Psi_k(z+L) = e^{ikL}\Psi_k(z). \tag{A5}$$

Real k correspond to propagating (traveling) Bloch modes, while complex k correspond to evanescent modes. Depending on the frequency ω, the full set of four Bloch eigenmodes in Eq. (A4) may include only propagating modes, only evanescent modes, or both. In any event, the respective set $[k_1,k_2,k_3,k_4]$ of four Bloch wave numbers satisfies the relation

$$[k_1,k_2,k_3,k_4]=[k_1^*,k_2^*,k_3^*,k_4^*]. \quad \text{(A6)}$$

Taking into account Eq. (A6), one can distinguish the following three possibilities.

(i) All four Bloch modes in Eq. (A4) are propagating

$$k_1=k_1^*, \quad k_2=k_2^*, \quad k_3=k_3^*, \quad k_4=k_4^*. \quad \text{(A7)}$$

(ii) All four Bloch modes in Eq. (A4) are evanescent. This is the case when the frequency ω falls into a photonic band gap. According to Eq. (A6), one can assume that in this case

$$k_1=k_2^*\neq k_1^*, \quad k_3=k_4^*\neq k_3^*. \quad \text{(A8)}$$

(iii) Two of the Bloch modes in Eq. (A4) are propagating modes, while the other two are evanescent. According to Eq. (A6), one can assume that in this case

$$k_1=k_1^*, \quad k_2=k_2^*, \quad k_3=k_4^*\neq k_3^*. \quad \text{(A9)}$$

In all cases, propagating modes with $u>0$ and evanescent modes with $k''>0$ are referred to as forward waves. The propagating modes with $u<0$ and evanescent modes with $k''<0$ are referred to as backward waves.

In reciprocal (nonmagnetic) periodic structures, the Bloch dispersion relation $\omega(k)$ is always symmetric with respect to the points $k=0$ and $k=\pi/L$ of the Brillouin zone

$$\omega(k_0+k)=\omega(k_0-k), \quad \text{where } k_0=0,\ \pi/L. \quad \text{(A10)}$$

In periodic structures composed of nonbirefringent layers, every Bloch wave is doubly degenerate with respect to polarization. A typical k-ω diagram for such a case is shown in Fig. 2(a). If, on the other hand, some of the layers display an in-plane anisotropy or gyrotropy, the polarization degeneracy can be lifted. The respective k-ω diagrams are shown in Fig. 3.

The speed of a traveling wave in a periodic medium is determined by the group velocity $u=\partial\omega/\partial k$. Normally, every spectral branch $\omega(k)$ develops stationary points (1), where the group velocity of the corresponding propagating mode vanishes. Usually, such points are located at the center and at the boundary of the Brillouin zone

$$k_s=k_0=0,\ \pi/L. \quad \text{(A11)}$$

This is always the case in periodic layered structures composed of nonbirefringent layers, where all stationary points coincide with photonic band edges, as shown in Fig. 2(a). If, on the other hand, some of the layers in a unit cell are birefringent, then in addition to Eq. (A11), some dispersion curves can also develop a reciprocal pair of stationary points corresponding to a general value of the Bloch wave number k, as shown in Fig. 3(b). The respective portion of the k-ω diagram can be described as a split band edge (SBE). The dispersion relation can develop a DBE or a SBE only if the periodic layered array has birefringent layers with misaligned in-plane anisotropy [13,23]. An example of such a layered structure is shown in Fig. 6.

Under normal circumstances, evanescent modes decay exponentially with the distance from the periodic structure boundaries. In such cases, the evanescent contribution to Ψ_T can be significant only in close proximity to the surface or some other defects of the periodic structure. The situation can change dramatically in the vicinity of a stationary point (1). At first sight, stationary points (1) relate only to propagating Bloch modes. But in fact, in the vicinity of every stationary point frequency ω_s, the imaginary part k'' of the Bloch wavenumber of at least one of the evanescent modes also vanishes. As a consequence, the respective evanescent mode decays very slowly, and its role may extend far beyond the photonic crystal boundary.

The final and most important remark is related to the EM eigenmodes in the vicinity of a DBE or such a RBE that is close in shape to a DBE. In either case, all four vector-columns (A1) corresponding to the four Bloch modes in Eq. (A4) are nearly parallel to each other (see the details in Refs. [12,13,23]). The latter circumstance is responsible for the giant EM field amplitude at the respective transmission resonance.

I. ENERGY FLUX: TRANSMISSION AND REFLECTION COEFFICIENTS

Let S_I, S_R, S_T, and S_P be the energy fluxes of the respective waves in Fig. 1. The transmission and reflection coefficients t and r are defined as

$$t=\frac{S_P}{S_I}, \quad r=-\frac{S_R}{S_I}. \quad \text{(A12)}$$

In the case of losses medium, the Poynting vector S is independent of z

$$S\equiv S_I+S_R=S_T=S_P.$$

In such a case $t=1-r=S/S_I$.

In the general case of the time-harmonic EM field $\Psi_T(z)$ being a superposition (A4) of several Bloch modes, propagating and/or evanescent, the contribution of each propagating mode Ψ_k to the total energy flux S is independent of others and can be expressed in terms of its group velocity and amplitude

$$S_k=W_k u_k, \quad \text{where } W_k\propto\langle|\Psi_k|\rangle^2. \quad \text{(A13)}$$

In the particular case of a single propagating mode, the quantity W_k in Eq. (A13) is equal to the energy density averaged over a unit cell L. By contrast, a single evanescent mode never transfers energy. Only a combination of forward and backward evanescent modes can contribute to the energy flux (see p. 327 in Ref. [12]).

2. ENERGY DENSITY AND ENERGY FLUX AT RESONANCE FREQUENCY

Consider the energy flux at transmission band edge resonance formed by a pair (A15) of reciprocal Bloch waves. Assume that the amplitude of the incident wave in Fig. 1 is unity and the transmission coefficient t in Eq. (A12) at resonance frequency is also of the order of unity. The boundary conditions (A3) together with Eq. (4) yield

$$\Psi_T(0)=\Psi_k(0)+\Psi_{-k}(0)\propto 1,$$

$$\Psi_T(D) = \Psi_k(D) + \Psi_{-k}(D) \propto 1. \tag{A14}$$

According to Eq. (A13), the energy flux associated with the time-harmonic field $\Psi_T(z)$ in Eq. (4) is

$$S = S_k + S_{-k} \approx W_k u(k) + W_{-k} u(-k) = (W_k - W_{-k}) u(k), \tag{A15}$$

where

$$W_k \propto \langle |\Psi_k|^2 \rangle, \quad W_{-k} \propto \langle |\Psi_{-k}|^2 \rangle.$$

Let us see under what conditions the finite resonance transmission is compatible with the vanishing group velocity in the vicinity of stationary point (1), where the transmission band edge resonance occurs. In the vicinity of stationary point (1), the magnitude $u(k)$ of the group velocity in Eq. (A15) is vanishingly small. The fact that the resonance energy flux remains of the order of unity implies that the amplitude of the Bloch components in Eq. (A15) increases so that

$$W_k - W_{-k} \propto u^{-1}, \quad \text{as } u \to 0. \tag{A16}$$

In order to reconcile the boundary condition (A14) with the requirement (A16) of a finite energy flux, we have to impose the following requirement on the amplitudes of the two Bloch components

$$W_k - W_{-k} \propto \sqrt{W_k} \propto u^{-1}, \quad \text{as } u \to 0. \tag{A17}$$

The relation (A17) was derived under the assumption that the time-harmonic filed $\Psi_T(z)$ inside the periodic medium is a superposition (4) of one forward and one backward propagating Bloch waves with equal and opposite wave numbers and group velocities. This is always the case for RBE related transmission resonance. However, the representation (4) is not applicable to the case of a DBE related giant resonance, because in this case the contribution of the evanescent modes is equally important [23]. Finally, in the case of SBE related transmission resonance, the relations (4) and (A17) may or may not apply, depending on whether the resonance field $\Psi_T(z)$ is formed by a single pair of propagating Bloch modes, or the contribution of all four propagating modes is equally important.

APPENDIX B: PHYSICAL CHARACTERISTICS OF THE PERIODIC LAYERED STRUCTURE USED IN NUMERICAL SIMULATIONS

The simplest periodic layered structure supporting a DBE or a SBE at normal propagation is shown in Fig. 6. A unit cell L contains one isotropic B layer and two misaligned anisotropic layers A_1 and A_2 with inplane anisotropy. The isotropic layers have the thickness B and the dielectric permittivity

$$\hat{\varepsilon}_B = \begin{bmatrix} \varepsilon_B & 0 & 0 \\ 0 & \varepsilon_B & 0 \\ 0 & 0 & \varepsilon_B \end{bmatrix}. \tag{B1}$$

The dielectric permittivity tensors $\hat{\varepsilon}_A$ in each anisotropic A layer has the form

$$\hat{\varepsilon}_A(\varphi) = \begin{bmatrix} \varepsilon_A + \delta\cos 2\varphi & \delta \sin 2\varphi & 0 \\ \delta \sin 2\varphi & \varepsilon_A - \delta \cos 2\varphi & 0 \\ 0 & 0 & \varepsilon_3 \end{bmatrix}, \tag{B2}$$

where the parameter δ characterizes the magnitude of inplane anisotropy, and the angle φ determines the orientation of the anisotropy axes in the x-y plane. All the A layers have the same thickness A and the same magnitude δ of inplane anisotropy. The only difference between the adjacent anisotropic layers A_1 and A_2 in Fig. 6 is their orientation φ. An important characteristic of the periodic structure in Fig. 6 is the misalignment angle

$$\phi = \varphi_1 - \varphi_2 \tag{B3}$$

between the layers A_1 and A_2. This angle determines the symmetry of the periodic array and, eventually, the kind of k-ω diagram it can display.

In all numerical simulations related to the periodic layered structure in Fig. 6 we use the following values of the material parameters in Eqs. (B1)–(B3)

$$\varepsilon_B = 16.0, \quad \varepsilon_A = 4.7797, \quad \delta = 3.4572, \quad \phi = \pi/6. \tag{B4}$$

At normal propagation, the numerical value of ε_3 in Eq. (B2) is irrelevant. The relative thickness of the A and B layers, can be different in different examples.

In all plots of the field distribution inside periodic media at $0 < z < D$ we, in fact, plotted the following physical quantity:

$$\langle |\Psi(z)|^2 \rangle = \langle \vec{E}(z) \cdot \vec{E}^*(z) + \vec{H}(z) \cdot \vec{H}^*(z) \rangle_L, \tag{B5}$$

which is the squared field amplitude averaged over a local unit cell. The actual function $|\Psi(z)|^2$, as well as the electromagnetic energy density distribution $W(z)$, are strongly oscillating functions of the coordinate z, with the period of oscillations coinciding with the unit cell length L. Given the relation $W \propto |\Psi(z)|^2$, the quantity (B5) can also be qualitatively interpreted as the smoothed energy density distribution, with the correction coefficient of the order of unity. In all plots, the distance z, the wavenumber k, and the frequency ω are expressed in units of L, L^{-1}, and cL^{-1}, respectively.

[1] L. Brillouin, *Wave Propagation and Group Velocity* (Academic, New York, 1960).
[2] L. D. Landau, E. M. Lifshitz, and L. P. Pitaevskii, *Electrodynamics of Continuous Media* (Pergamon, New York, 1984).
[3] J. Joannopoulos, R. Meade, and J. Winn, *Photonic Crystals* (Princeton University Press, Princeton, 1995).
[4] A. Yariv and Pochi Yeh, *Optical Waves in Crystals* (Wiley-Interscience, New York, 1984).
[5] Pochi Yeh, *Optical Waves in Layered Media* (Wiley, New York, 1988).
[6] Weng Cho Chew, *Waves and Fields in Inhomogeneous Media* (Van Nostrand Reinhold, New York, 1990).
[7] M. Notomi, Phys. Rev. B **62**, 10696 (2000).
[8] A. Figotin and I. Vitebskiy, Phys. Rev. B **67**, 165210 (2003).
[9] A. Figotin and I. Vitebskiy, Phys. Rev. E **68**, 036609 (2003).
[10] J. Ballato, A. Ballato, A. Figotin, and I. Vitebskiy, Phys. Rev. E **71**, 036612 (2005).
[11] A. Figotin and I. Vitebskiy, J. Magn. Magn. Mater. **300**, 117 (2006).
[12] A. Figotin and I. Vitebskiy, Waves Random Media **16**, 293 (2006).
[13] A. Figotin and I. Vitebskiy, Phys. Rev. E **74**, 066613 (2006).
[14] A. Figotin and V. Gorentsveig, Phys. Rev. B **58**, 180 (1998).
[15] A. Vinogradov, A. Dorofeenko, S. Erokhin, M. Inoue, A. Lisyansky, A. Merzlikin, and A. Granovsky, Phys. Rev. B **74**, 045128 (2006).
[16] M. Selim Unlu and S. Strite, J. Appl. Phys. **78**, 607 (1995).
[17] J. Dowling, M. Scalora, M. Bloemer, and Ch. Bowden, J. Appl. Phys. **75**, 1896 (1994).
[18] M. Scalora, J. Flynn, S. B. Reinhardt, R. L. Fork, M. J. Bloemer, M. D. Tocci, C. M. Bowden, H. S. Ledbetter, J. M. Bendickson, J. P. Dowling, and R. P. Leavitt, Phys. Rev. E **54**, R1078 (1996).
[19] M. Bloemer, Myneni, M. Centini, M. Scalora, and G. D'Aguanno, Phys. Rev. E **65**, 056615 (2002).
[20] M. Soljacic, S. Johnson, S. Fan, M. Ibanescu, E. Ippen, and J. D. Joannopoulos, J. Opt. Soc. Am. B **19**, 2052 (2002).
[21] J. Poon, J. Scheuer, Y. Xu, and A. Yariv, J. Opt. Soc. Am. B **21**, 1665 (2004).
[22] S. Yarga, G. Mumcu, K. Sertel, and J. Volakis (unpublished).
[23] A. Figotin and I. Vitebskiy, Phys. Rev. E **72**, 036619 (2005).